5.8 Biological Science II

Biological research activities, other than protein crystallography, are exploiting various methodology using synchrotron radiation. Followings are the typical research results obtained with small angle scattering, fibre diffraction and irradiation experiment for radiobiology. These results have contributed very much in photobiology, biophysics and radiobiology.

Light-Induced Conformational Change of Photoactive Yellow Protein

Photoactive yellow protein (PYP), a photoreceptor protein found in the purple phototrophic bacterium, *Ectothiorhodospira halophila,* acts as a blue-light receptor for the negative phototaxis of the bacterium. The chromophore of PYP, a thioester-linked trans-*p*-coumaric acid, is isomerized to the *cis*-form upon photon absorption and PYP undergoes a photocycle. Among the photocycle intermediates, the last one (PYPM), whose absorption band is located in the near-UV region, is considered to be in a physiologically active form. The structure of PYPM has been analyzed by time-resolved crystallography [1]. The structural difference between PYP and PYPM in the crystal form is limited to the region around the chromophore. However, accumulated evidence strongly suggests that the structural change under physiological conditions is much larger than that in the crystal, probably because conformational change is restricted in the crystal. We have examined the light-induced conformational change of PYP in solution by small-angle X-ray scattering (SAXS) [2].

PYP was heterologously overexpressed by *Escherichia coli*, and reconstituted by adding p-coumaric anhydride. Because of the short lifetime of PYP_M (~100 ms), its characterization is difficult. To stabilize PYP_M, the N-terminal 6, 15 or 23 amino acid residues of PYP were truncated by bovine pancreas chymotrypsin (T6, T15 and T23, respectively). Systematic characterization of the truncated PYPs provided information on the structural change in the N-terminal region. The SAXS measurements were carried out at BL-10C.

The square of the radius of gyration (R_g^2) of PYPs in the dark was estimated by a Guinier plot (Fig. 1). Values of R_g^2 for T6, T15, and T23 under illumination (T6M, T15M, and T23M) were similarly estimated. The R_g^2 values for the dark states were slightly decreased by truncation. Upon illumination, the R_g values of truncated PYPs were markedly increased. The increase in R_g by illumination was 1.1 Å for T6 and 0.7 Å for T15 and T23. It should be noted that the difference in R_g between T6 and T15was 0.3 Å, but that between T6M and T15M it was 0.7Å. In contrast, the difference in R_g between T15 and T23 was 0.6 Å for both dark and light conditions. Namely, the decrease of R_g by removal of Gly7-Leu15 in the M state was larger than that in the dark state, but that of Ala16- Leu23 was constant. Therefore, Gly7-Leu15 in T6M is more responsible for R_g than it is in T6. This means that Gly7-Leu15 in the dark state is located more proximately to the center than in the M intermediate. In the dark state, Gly7-Leu15 forms a short α-helix which lies parallel to the plane of the β-sheet (Fig. 2). The present data can be explained by a model in which the N-terminal loop is detached from the β-sheet upon the formation of PYP_M. The structural change for formation of PYP_M is not merely a rearrangement of the surface charge distribution but involves a global conformational change, resulting in increases in the dimensions and changes in the shape. This may enable the interaction with other molecules such as membrane and proteins.

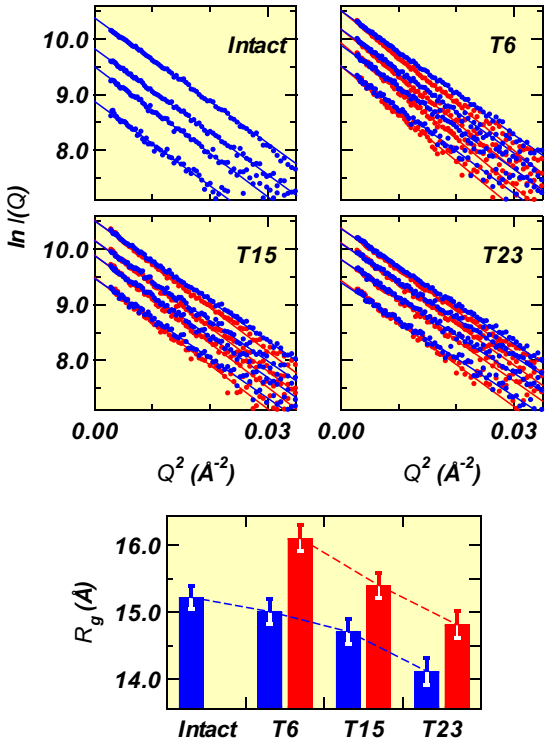

Figure 1
Guinier plots of intact PYP, T6, T15, and T23 in the dark (blue) and under continuous illumination with >410 nm light (red). The protein concentrations were 10, 6, 4, and 2 mg/ml (from top to bottom) for intact PYP, 12, 8, 6, and 4 mg/ml for T6 and T15, and 10, 8, 6, and 4 mg/ml for T23. Bottom panel; Comparison of R_g in the dark (blue) and with light (red).

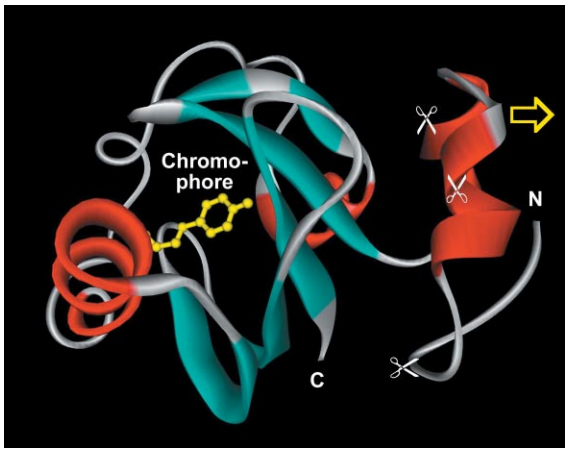

Figure 2
Structure of PYP in the dark (PDB: 2PHY). Chromophore is colored in yellow. Chymotrypsin-cleavage sites are shown by scissors. The present experiment suggested that N-terminal loop is detached from the β-sheet upon formationof PYP_M.

Energy Transducing Conformation Changes of Myosin Motor Proteins

Elucidating the mechanism by which the actin-myosin motor system transduces the chemical energy of ATP hydrolysis to power the movement of animals and cells remains one of the major challenges in biological science. Skeletal muscle myosin (myosin II) consists of two globular heads linked by helical segments that supercoil to form a long helical rod. The rod segments assemble into the shaft of the myosin filaments, and the head portions project outward towards the actin filaments, forming the cross-bridges that are responsible for the generation of a sliding force between the two filaments. Myosin heads play a key role in converting chemical energy in the form of ATP into mechanical energy driving the directional motion of myosin heads relative to the actin filaments. It has long been expected for the cross-bridge mechanism of the acto-myosin motor system that global conformational changes of myosin heads interacting with actin occur in coupling with an ATP hydrolysis reaction. Prior to X-ray crystallographic studies, X-ray solution scattering of isolated myosin heads (subfragment 1, S1) first indicated that the long α-helical regulatory domain containing two light chains deformed globally relative to its catalytic domain during the ATPase cycle [3]. The deformation involves both a tilt and a twist, resulting vectorially in a 5-nm spinning of the distal end of the regulatory domain (Fig. 3) [4,5].

Recently, X-ray scattering studies of S1s with various nucleotide analogs mimicking the reaction steps along the ATPase cycle of S1 have been performed at the Photon Factory small-angle X-ray scattering beamline. The data showed that S1 has distinctly different conformations in the presence of various analogs, implying that the myosin heads alter their conformation depending upon the bound nucleotides (Fig. 4) [6-9]. As summarized in Fig. 4, a large conformational change of the regulatory domain of S1 occurs in a lever arm-like fashion both in the S1*.ATP and $S1^{+}$.ADP states before

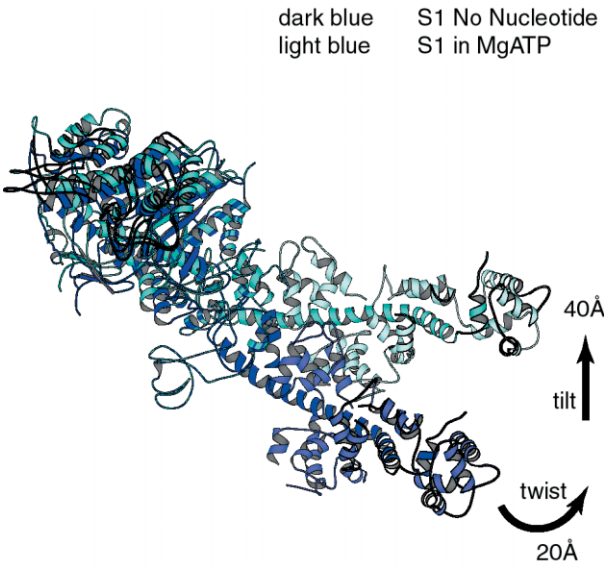

Figure 3
The global conformational change of the myosin head (S1) during energy transduction. The motion of the light chain binding domain of S1 involves a tilt and a slew. The S1 molecule is shown with is catalytic domain facing the actin filament axis.

and after the key intermediate state (S1**.ADP.Pi) of its ATPase cycle. The direction of motion of the regulatory domain is opposite to that occurring in the S1**.ADP.Pi state. When an actin filament is present, the contractile or sliding force is thought to be produced in the transition from an S1**.ADP.Pi state to an $S1^{+}$.ADP state, that is, in the phosphate release step. The present results may indicate a working stroke of myosin heads amounting to ca. 10 nm in this transition. Recent X-ray crystallographic analysis of S1s from invertebrate muscle myosin with various nucleotide analogs has suggested the possible atomic mechanism of such a global movement of the regulatory domain. Support for such a lever arm hypothesis for the motor action of myosin heads is found in recent time-resolved X-ray diffraction and quick-freezing electron microscopic studies from contracting muscle fibers. On the other hand, we have stressed that the elastic dynamics of thin actin filaments

state	S1 ⇌ S1. ATP ⇌ S1*. ATP ⇌ S1**. ADP. Pi ⇌ S1†. ADP ⇌ S1. ADP					
sample	S1 no nucleotide	S1+MgAMPPNP S1+MgPPi	S1.ADP-*p*PDM	S1+MgATP (~20°C)	S1+MnATP (~4°C)	S1+MnADP (~4°C) S1+MgADP (~20°C)
Rg(Å)	47.8±0.2	48.4±0.1	50.7±0.4	45.7±0.8	51.4±0.6	48.1±0.2
Dmax(Å)	~160	~160	~170	~150	~170	~155
model		0 nm	5 nm	10 nm	10 nm	5 nm

Figure 4
Global motion of the light chain binding domain of S1 with various nucleotide analogs mimicking the intermediate steps of the myosin ATPase reaction. The radius of gyration value (Rg) and the maximum chord length (D_{max}) of S1 with and without nucleotides were obtained respectively from Guinier plots and the p(r) functions of the X-ray solution scattering data. The top row of the table shows the representative intermediate states along the ATPase reaction of S1. The movement direction and magintudes of the distal and of the light chain binding domain are shown with an arrow and a value relative to the S1 with no nucleotide of the S1. ATP state in each transition of the states in the bottom row of the table. In the second row AMPNP is adenyllimidodiphosphate, PPi is pyrophosphate and S1. ADP- *p*PDM is an S1 trapping ADP by *p*PDM (*p*-phenylenedimaleimide) which croslinks two reactive Cysteine resdues (SH1 and SH2) of S1.

is important for the acto-myosin motor activity under the action of myosin heads [10]. Coordinated conformational changes of actin and myosin are clearly required to perform efficient energy transduction in the acto-myosin motor system.

Equilibrium and Kinetics of the Allosteric Transition of the Chaperonin GroEL Studied by Solution X-Ray Scattering

The GroEL from *Escherichia coli*, a tetradecameric protein complex of 14 identical 57-kDa subunits arranged in two heptameric rings stacked back-to-back with a central cavity, is one of the best characterized molecular chaperones (Fig. 5). The ATP-dependent control of the affinity of GroEL for its target protein and the resulting facilitation of protein folding are underpinned by the allosteric transitions of GroEL induced by ATP. However, these allosteric transitions have so far only been investigated by the ATPase assay of GroEL or by fluorescence spectroscopy of tryptophan mutants of GroEL, and there is no direct structural data for the real-time allosteric transitions in solution. Therefore, a number of mysteries remain unsolved, especially concerning the structural characteristics and the kinetics of the allosteric transitions. Another method, which can monitor directly the global structural changes of the protein molecule in real time, is certainly required if we are better to understand the allosteric mechanisms of GroEL.

Small-angle X-ray scattering (SAXS) is a powerful technique for studying directly any changes in the size and shape of a protein molecule and a protein complex in solution, and this technique should complement the structural information acquired via other spectroscopic (fluorescence, circular dichroism, etc.) techniques and via enzymatic assay. Recently, the use of synchrotron radiation has made it possible to combine a stopped-flow technique with SAXS measurements. Furthermore, combination of the SAXS technique with a two-dimensional (2D) charge-coupled device (CCD)-based X-ray detector has made it possible to improve the signal-to-noise (S/N) ratio of the stopped-flow SAXS data dramatically. This new technique should be useful for investigating the allosteric transitions of large protein complexes [11,12]. In the present study, we have investigated the ATP induced allosteric transitions of GroEL with static and stopped-flow SAXS [13,14]. The results of the SAXS measurements show that the three

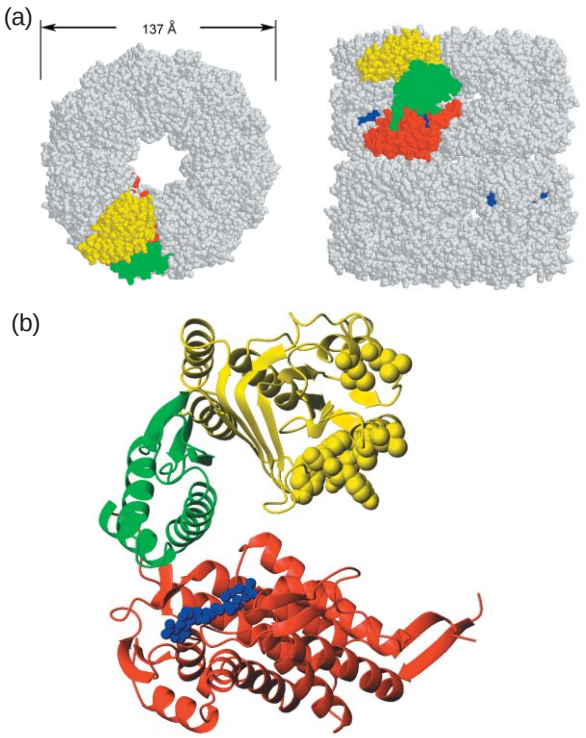

Figure 5
X-ray crystallographic structure of GroEL (PDB: 1KP8). (a) The 14-mer structure the top view (left) and the side view (right). (b) The structure of a single subunit. The apical (yellow), intermediate (green) and equatorial (red) domain areshown. The nucleotide (ATPγS) is shown in blue.

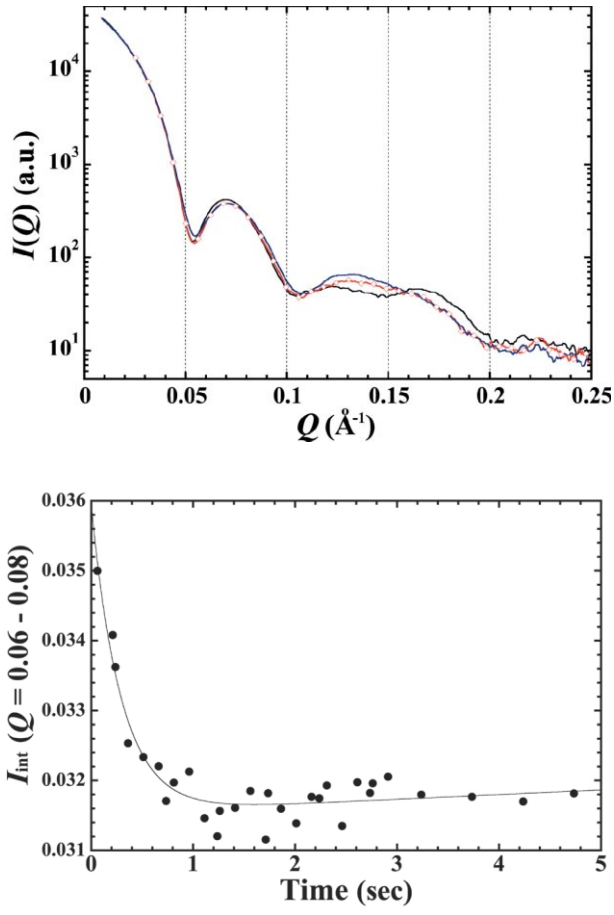

Figure 6
(a) SAXS patterns of GroEL at 0 M (TT) (black line), 85 μM (TR)(red line with open circles), and 3 mM ATP (RR) (blue line) at 25°C. The scattering intensity *I(Q)* is shown as a function of *Q*. (b) Kineticcurve of the ATP-induced structural change of GroEL at 4.8°C monitored by integral intensity, I_{int}. The integral region of Q employed was from 0.06 $Å^{-1}$ to 0.08 $Å^{-1}$. The structural change was initiated by mixing with ATP (fi nal concentrations of 3.8 μ M (3 mg/ml) and 85 μM for GroEL and ATP, respectively). The solid line is a theoretical kinetic progress curve assuming a single exponential with the equation: $I_{int}(t) = Ae^{-kt} + Bt + C$, where A and k are the amplitude and the rate constant of the exponential phase and *B* and *C* are constants. The second term *Bt* is introduced for the purpose of correcting for the linear increase in the scattering intensity caused by beam damage.

allosteric states (the TT, the TR, and the RR states) are structurally different from each other (Fig. 6(a)); the two rings of GroEL assume two allosteric states, T (tense) and R (relaxed), depending on ATP concentration, and hence there are three allosteric states, TT, TR and RR, for the GroEL particle. The kinetics of the TT to TR transition has been observed for the first time directly using stopped-flow SAXS. The rate constant of the transition is 3.4 s^{-1} (85 μM ATP and 4.8ºC) (Fig. 6(b)), and hence this is shown to correspond to the second phase of the ATP-induced kinetics of tryptophan-inserted GroEL previously measured by stopped-flow fluorescence. We have also found by fluorescence spectroscopy that the first phase is a bimolecular process caused by non-cooperative binding of ATP to GroEL with a bimolecular rate constant of 5.8×10^{-5} $M^{-1}s^{-1}$. The ATP-induced co-operative transition observed by fluorescence as well as SAXS measurements at low concentration of ATP (< 400 μM) is well explained by a kinetic Monod-Wyman-Changeux (MWC) model that is a combination of the conventional transition state theory and the basic MWC model.

Three Conformations of the MutS Protein Regulated by Adenine Nucleotides

In living organisms, DNA is continuously being damaged as a result of errors introduced by DNA replication, genetic recombination or other processes [15]. These DNA lesions may lead to mutations, genetic diseases and tumors. To remove such DNA lesions, all organisms have developed various DNA repair systems, including the DNA mismatch repair (MMR) system. It has been shown that MutS protein (about 90 kDa) recognizes and binds specifically to mismatched base pairs in DNA, constituting the first step of MMR [15, 16]. Then, MutL and other proteins cooperate in subsequent steps to complete the MMR pathway. The pathogenic genes of human hereditary non-polyposis colorectral cancer (HNPCC) appear to share a high degree of homology with bacterial MutS and MutL. Moreover, MutS homologues have also been isolated from plants. These observations suggest that the MMR system is essential for all living organisms from bacteria to eukaryotes. MutS has a weak ATP hydrolysis activity for which no role has yet been identified. However, recent reports underscore the importance of ATP for the function of these proteins, since ATP and its poorly hydrolyzable analogue, ATPγS [adenosine-5'-O-(3-thiotriphosphate)], can affect the DNA binding activity of MutS.

Small-angle X-ray scattering (SAXS) is a powerful technique for measuring the size and general shape of molecules in solution [17]. SAXS measurements of MutS were performed at BL-10C both in the presence and in the absence of adenine nucleotides. The results demonstrate the existence of three different conformations of MutS in solution: ATP-bound, ADP-bound and nucleotide-free forms. The ATP-bound form has the most compact conformation with a maximum particle dimension (d_{max}) of max 110 Å and with a radius of gyration (R_g) of 37 Å. The ADP-bound form has the most stretched conformation with a d_{max} of 130 Å and an R_g of 44 Å. The nucleotide-free form shows values intermediate between the two forms (120 Å for d_{max} and 41 Å for R_g). These conformational changes induced by adenine nucleotides have been confirmed by an analysis of the distance distribution function (P(r)). Recently, methods for reconstructing three-dimensional density maps of macromolecules in solution have been developed [18]. By using these techniques, the shapes of MutS in solution under various conditions were calculated. In the structure models, one axis of the molecule is longer than the other, and a hole is present in the lower part (Fig. 7). The rendering of the three-dimensional density maps shows three different conformations for MutS bound to different nucleotides. The shapes of the model structures differ from each other, especially in the upper region. When bound to ADP, the molecule appears to have two holes (Fig. 7b). This is similar to the crystallographic structure which clearly displays two holes (Fig. 7d). In the latter, the upper hole is occupied by bound DNA [19]. An open/close movement of the upper region may occur by binding of adenine nucleotides, consequently modulating the DNA binding activity of MutS. We have also demonstrated that a MutS mutant, in which a lysine belonging to the nucleotide binding motif is replaced by an alanine, can not undergo conformational changes. Based on these findings, we conclude that the DNA-binding activity of MutS may depend on conformational changes triggered by both the binding and hydrolysis of ATP [20].

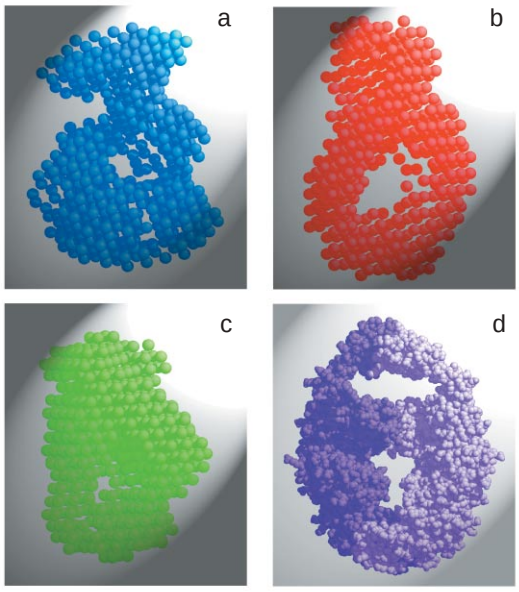

Figure 7
Simulated models of the three-dimensional structure for MutS in solution. The shapes of nucleotide free (a), ADP bound (b) and ATP bound (c) forms were calculated from the P(r) functions. (d) shows the space filling model of E. coli MutS dimer, in which the bound DNA was removed from the MutS-DNA complex of the crystal structure (PDB accession number 1E3M).

Enhancement of X-ray-Induced DNA Damage with DNA Bound Molecules Containing Platinum

– Possible Application to Radiotherapy –

High energy photons induce various kind of DNA damage. The damage is derived from ionization and excitation of DNA itself or of surrounding materials such as water molecules. If a photon induces innershell ionization, Auger processes follow in the biological molecules, and the ejected electrons and/or multiply charged ion might induce breakage of chemical bonds. The underlying idea is that the Auger effect could contribute a great deal to radiotherapy when the target molecule is selectively introduced into neoplastic tissues to preferentially kill tumor cells. A compound having a relatively heavy atom would be a candidate target molecule for radiotherapy, because of its large X-ray absorption coefficient. In this study, we adopted one of the platinum-containing molecules, chloroterpyridine platinum II (PtTC) (Fig. 8), which binds to DNA, and examined the possibility of its application to radiotherapy. Figure 3 shows an absorption spectrum of PtTC around the LIII absorption edge of platinum. A resonant structure near the LIII edge was observed with its maximum located at E_{res} = 11562 eV. Irradiation with monochromatic X-rays at the resonance energy was performed at BL-27B.

Covalently closed circular DNA, pBR322 plasmid DNA, was used as a biological sample. The DNA solution was mixed with the PtTC solution to the ratio of the number of Pt atoms to the number of phosphorus atoms in DNA of 1/10, namely, one platinum atom in every 5 base-pairs in DNA. After irradiation, the numbers of single- and double-strand breaks were measured by a gel electrophoresis method. In this report, we focused mainly on DNA double strand breaks (DSBs), one of the most crucial kinds of DNA damage induced by ionizing radiation.

The numbers of DSBs per DNA molecule were plotted (Fig. 9) as a function of radiation dose under different conditions as below;

(1) in the presence and absence of PtTC (curves A and B) irradiated at the platinum LIII resonance absorption energy (E_{res} = 11562 eV)

(2) as above but in the presence of a radical scavenger, dimethyl sulfoxide (DMSO), to estimate the contribution

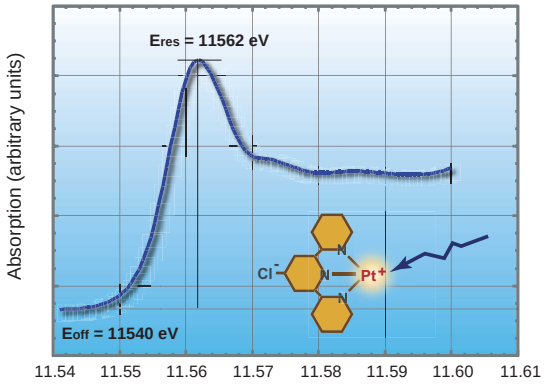

Figure 8
Molecular structure and X-ray absorption spectrum of PtTC.

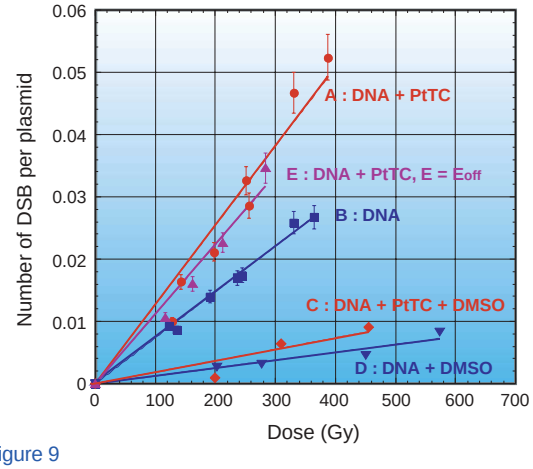

Figure 9
DSBs per plasmid induced with monochromatic X-rays.

of radical mediated damage (curves C and D)

(3) in the presence of PtTC irradiated off-resonance (E_{off}= 11540 eV) (curve E)

Enhancement of the DSB induction was observed when the plasmids contained PtTC. Even when off-resonant X-rays were used, DSB yields were higher than expected based upon the absorption cross section (for detail of the quantitative analysis, see ref. [21]). In addition, more than 85% of DSBs were scavengable by DMSO, which means more than 85% of DSBs were mediated by water radicals in the presence of PtTC. From these results, a mechanism could be suggested that the photoelectrons generated from the ionization of water efficiently ionize platinum atoms. Since the heavy atoms have a large collision cross section with electrons, these atoms located close to DNA likely behave as a radiosensitizer, and hence the DNA-binding compounds containing heavy atoms have the potential to be a radiosensitizer in radiotherapy for the treatment of tumors. Recently, we started an experiment with mammalian cells in order to demonstrate the potentiality of PtTC. Figure 10 displays the surviving fraction of Chinese hamster ovary (CHO) cells cultured in the medium supplemented with and without PtTC, irradiated at the resonant energy. An enhancement was clearly

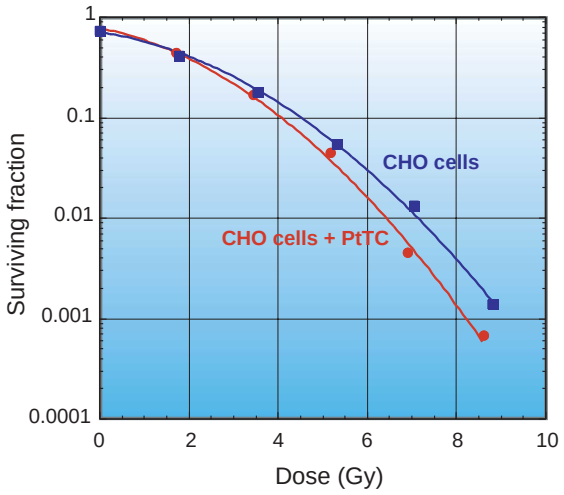

Figure 10
Surviving fraction of CHO cells irradiated at the platinum L_{III} resonance energy.

observed. This result indicates that this drug might be applicable to radiotherapy of tumors.

References

[1] U. K. Genick, G. E. Borgstahl, K. Ng, Z. Ren, C. Pradervand, P. M. Burke, V. Srajer, T. Y. Teng, W. Schildkamp, D. E. McRee, K. Moffat and E. D. Getzoff, *Science,* **275** (1997) 1471.

[2] Y. Imamoto, H. Kamikubo, M. Harigai, N. Shimizu and M. Kataoka, *Biochemistry,* **41** (2002) 13595.

[3] K. Wakabayashi, M. Tokunaga, I. Kohno, T. Hamanaka, Y. Takezawa, T. Wakabayashi and Y. Amemiya, *Science,* **258** (1992) 443.

[4] Y. Sugimoto, M. Tokunaga, Y. Takezawa, M. Ikebe and K. Wakabayashi, *Biophys. J.,* **68** (1995) 29S.

[5] Y. Sugimoto and K. Wakabayashi, Protein, *Nucleic Acid, Enzyme*, **44** (1999) 1605.

[6] Y. Sugimoto, M. Tokunaga and K. Wakabayashi, *Photon Factory Activity Report 1996,* #**14** (1997) 334.

[7] Y. Sugimoto, T. Okumura, T. Arata, Y. Takezawa and K. Wakabayashi, *Photon Factory Activity Report 2000,* #**18** (2001) B233.

[8] T. Okumura, T. Arata, Y. Sugimoto, Y. Takezawa, M. Kiyotoshi and K. Wakabayashi, *Photon Factory Activity Report 2001,* #**19** (2003) B203.

[9] Y. Sugimoto et al., to be published.

[10] Y. Takezawa, Y. Sugimoto and K. Wakabayashi, *Photon Factory Activity Report 2000,* #**18** (2001) A41.

[11] K. Ito and Y. Amemiya, *J. Jpn. Soc. Synchrotron Rad. Res.* **13** (2000) 372 (in Japanese).

[12] M. Arai, K. Ito, T. Inobe, M. Nakao, K. Maki, K. Kamagata, H. Kihara, Y. Amemiya and K. Kuwajima, *J. Mol. Biol.,* **321** (2002) 121.

[13] T. Inobe, M. Arai, M. Nakao, K. Ito, K. Kamagata, T. Makio, Y. Amemiya, H. Kihara and K. Kuwajima, *J. Mol. Biol.,* **327** (2003) 183.

[14] T. Inobe, K. Kikushima, T. Makio, M. Arai and K. Kuwajima, *J. Mol. Biol.,* **329** (2003) 121.

[15] E.C. Friedberg et al., *DNA Repair and Mutagenesis. ASM Press, Washington, D.C.* (1995).

[16] P. Modrich, *Ann. Rev. Genet.,* **25** (1991) 229.

[17] O. Glatter and O. Kratky, *Small Angle X-ray Scattering. Academic Press, New York* (1982).

[18] D.L. Svergun, *Biophisical J.,* **76** (1999) 2879.

[19] M.H. Lamers et al., *Nature,* **407** (2000) 711.

[20] R. Kato et al., *J. Mol. Biol.,* **309** (2001) 227.

[21] K. Kobayashi, H. Frohlich, N. Usami, K. Takakura and C. Le Sech, *Radiat. Res.*, **157** (2002) 32.